ACS OMEGA

Open Access

This article is licensed under CC-BY-NC-ND 4.0

http://pubs.acs.org/journal/acsodf

Article

Hydroxyethylcellulose-Directed Synthesis of Gold Microplates with Hydrogen Peroxide in an Aqueous Phase

Linlin He, Bo Shen, Yu Ren, Huaming Mao, Jungang Yin, Wei Dai, Shuanglong Zhao, and Hongwei Yang*

Cite This: *ACS Omega* 2024, 9, 8789−8796

Read Online

ACCESS | Metrics & More | Article Recommendations | Supporting Information

ABSTRACT: In this study, we successfully synthesized well-defined polygonal gold microplates for the first time in an aqueous phase using hydroxyethylcellulose (HEC) in the presence of hydrogen peroxide (H_2O_2). HEC played a pivotal role during the synthesis, acting not only as a biotemplate but also as an in situ reduction site for the nucleation and growth of gold (Au) microplates. H_2O_2 played a crucial role in accelerating the growth of Au microplates from the Au nucleus. This methodology is ecofriendly and easy to operate and has potential applications in various fields, such as electronics, photonics, and biotechnology.

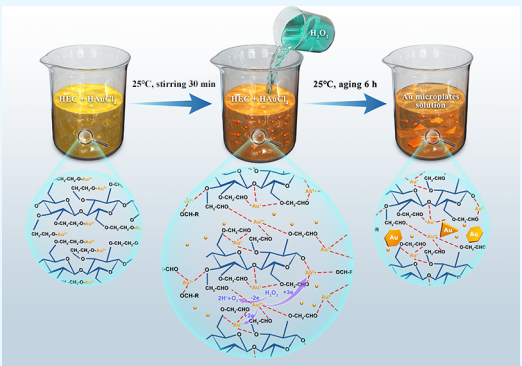

INTRODUCTION

Gold (Au) nano/microplates have been extensively investigated because of their remarkable physical and chemical properties, including high surface-to-volume ratio, surface plasmon resonance, and superior biocompatibility.[1,2] These attributes make Au nano- and microplates highly versatile for a wide spectrum of applications in electronics, photonics, and biotechnology. In biotechnology, Au nano/microplates have been employed in biomolecules and pathogen detection,[3] drug delivery,[4] and photothermal therapy.[5] They have emerged as fundamental components for producing plasmonic devices[6] and microelectrodes in electronics,[7] whereas they have been used to create high-efficiency solar cells and serve as nanoantennas for light harvesting and sensing in photonics.[8] Consequently, the synthesis of Au nano/microplates has attracted significant attention in recent years owing to their potential for diverse applications across various fields.

To date, various synthetic techniques have been employed to produce Au nano/micrometer-sized structures, including chemical reduction,[9] seed-mediated growth,[10] photochemical methods,[11] template-assisted growth,[12] and green synthesis methods.[13] For instance, Yu et al. successfully synthesized Au nanosheets by reacting $HAuCl_4$ with branched polyethylenimine (BPEI) in the presence of urea. Structural characterization showed that the average lateral size of the synthesized Au nanosheets was 2−8 μm, with a thickness of approximately 40 nm.[14] Miranda and co-workers synthesized triangular nanosheets in an aqueous solution based on the reduction of Au salt using tin(IV) porphyrin as a photocatalyst. Cetyltrimethylammonium bromide (CTAB) served as the stabilizer, whereas triethanolamine (TEA) acted as the final electron donor. By changing the concentration of CTAB, the average edge length of the triangular nanosheets could be changed in the range of 45−250 nm.[15] Kida developed a new route to obtain two-dimensional Au nanostructures. The author leveraged chloroaurate ions ($AuCl_4^-$) at the two-dimensional interface between water and chloroform using an amphiphilic polyoxometalate and dimethyloctadecylammonium as a hybrid photocatalyst under UV irradiation in air at room temperature. Large single-crystal gold nanosheets (lateral dimension, approximately 20 μm; thickness, approximately 150 nm) were produced eventually.[16] Safavi and his colleagues also confirmed that the Au nanosheet has the potential to build a self-assembled structure at the water/toluene interface through the molecular dynamic simulation of the toluene/Au nanosheet/water system.[17]

As stated above, some conventional templates, reducing agents, and solvents used for the synthesis of Au nano/microplates have been shown to be toxic and harmful to the environment and human health. In addition, the production of traditional reducing agents and solvents involves expensive and energy-intensive processes. Moreover, the use of conventional methods can adversely affect the functionality and biocompat-

Received: August 15, 2023
Revised: November 22, 2023
Accepted: December 21, 2023
Published: February 14, 2024

© 2024 The Authors. Published by American Chemical Society

https://doi.org/10.1021/acsomega.3c06039
ACS Omega 2024, 9, 8789−8796

ibility of the synthesized Au microplates. Conversely, although the micrometer-sized Au plates offer distinct advantages in practical applications over nanosheets within certain domains such as electronic paste, coating, and photonics, it has become evident that there is a scarcity of research on the synthesis and growth mechanism of Au microplates, especially when compared with those of Au nanoplates. Therefore, there is an urgent need to develop sustainable and environmentally friendly approaches for the synthesis of Au microplates to overcome these limitations and enhance the efficiency, functionality, and biocompatibility of Au microplates for potential applications in diverse fields.

In this study, we present a novel achievement in the synthesis of highly uniform polygonal Au microplates in an aqueous phase with the aid of HEC and H_2O_2. In particular, the effects of HEC and H_2O_2 on the synthesis of Au microplates are systematically investigated, and a possible nucleation and growth mechanism is proposed.

METHODS

Tetrachloroauric acid tetrahydrate ($HAuCl_4{\cdot}4H_2O$, 47.8%) and hydrogen peroxide (H_2O_2, 30% w/w) were purchased from Sichuan Xilong Chemical Co., Ltd. Hydroxyethyl cellulose (HE, HS 100000 YP2, viscosity= 100,000 mPa·s) was obtained from Sansheng Chemical Co., Ltd. All chemicals were used as received without further purification, and deionized water with a resistivity of not less than 18.2 MΩ·cm was used in all the aqueous phase experiments.

Synthesis of Au Microplates. Au microplates were synthesized from $HAuCl_4$ in the aqueous phase in the presence of HEC and H_2O_2. Typically, in a 25 mL beaker were placed HEC, tetrachloroauric acid tetrahydrate ($HAuCl_4{\cdot}4H_2O$, 47.8%), and deionized water. The mixture was stirred for 45 min. Subsequently, 30% w/w H_2O_2 was added, and stirring continued for 30 min. The solution was left undisturbed at room temperature for 6 h. The yellowish micelle solution turned into a distinctly silky-orange micelle solution, indicating the generation of Au microplates. The Au microplates were then washed several times with hot deionized water and stored in an ethanol suspension.

Characterization. The morphology and microstructure analyses of the Au microplates were conducted using scanning electron microscopy (SEM, JEOL JSM-6510A) and transmission electron microscopy (TEM, JEM-2100) under a high vacuum of 20 kV. The phase identification of the Au microplates was performed by X-ray diffraction (XRD, Rigaku D/MAX-3B) with a Cu target and Kα radiation (λ = 1.54056 Å). The XRD pattern was collected across the range of 2θ values from 35 to 90° with a scanning step size of 0.02°. A UV−vis spectrophotometer (PERSEE Genera TU-1901) was used to monitor the evolution of the UV−vis spectra of the gold microplates. The solid-phase FTIR spectra of the HEC and HEC-Au microplates obtained after drying at 303 K before the reaction were acquired using a liquid IR pool and FTIR beam (Bruker IFS 66 v/s). Raman spectroscopy (inVia) was used to analyze the vibrational motion and transition of the aqueous systems of the HEC and HEC-Au microplates. The NMR (^{1}H NMR) spectra of all the HEC polymer−metal nanocomposites were acquired using a Bruker Avance Neo 600 spectrometer operating at 600 MHz for ^{1}H NMR. To prepare the NMR samples, the materials were dissolved in heavy water (D_2O).

RESULTS AND DISCUSSION

SEM was used to elucidate the morphologies of the prepared samples, and the results are shown in Figure 1. In Figure 1a,

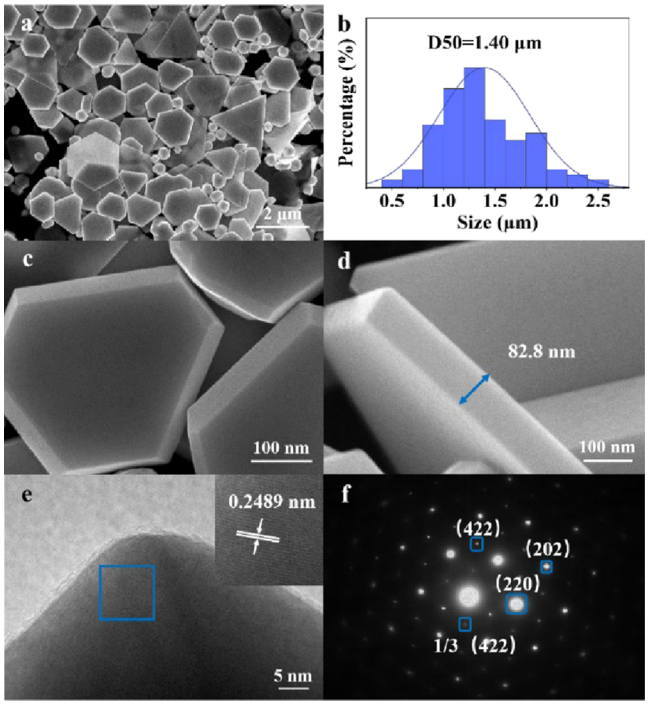

Figure 1. (a) Low-magnification SEM image of gold microplates synthesized at 298 K after 6 h with 3.6 mM of $HAuCl_4$ solution, 0.8% (w/v) of HEC solution, and 0.83 mM of H_2O_2 solution, respectively. (b) Statistical histogram of the lateral size of gold microplates. (c, d) High-magnification SEM of gold microplates. (e) HRTEM image of single gold microplates. (f) SAED pattern of gold microplates.

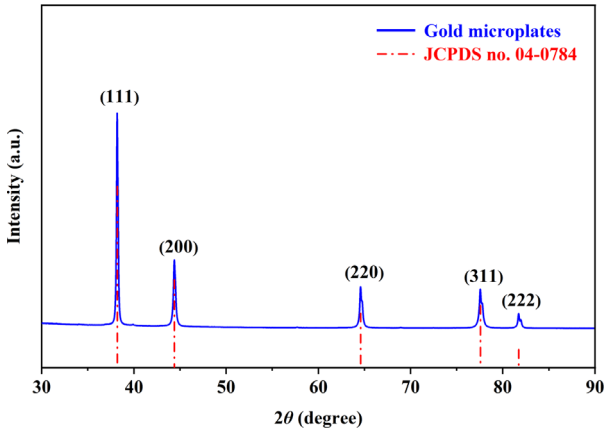

Figure 2. XRD pattern of the gold microplates.

many micrometer-sized plate-like structures of various shapes, such as triangles, truncated triangles, hexagons, and polygons, are shown, located on the Si substrate. Figure 1b shows the statistical distribution of the lateral size obtained from nonrepetitive SEM images of 200 microplates, which reveals that the microplates have an average diameter of 1.4 μm. With higher magnification in Figure 1c−e, it is clear that the Au microplates have well-defined boundaries with a thickness of approximately 80 nm. The lattice structure is also visible,

https://doi.org/10.1021/acsomega.3c06039
ACS Omega 2024, 9, 8789−8796

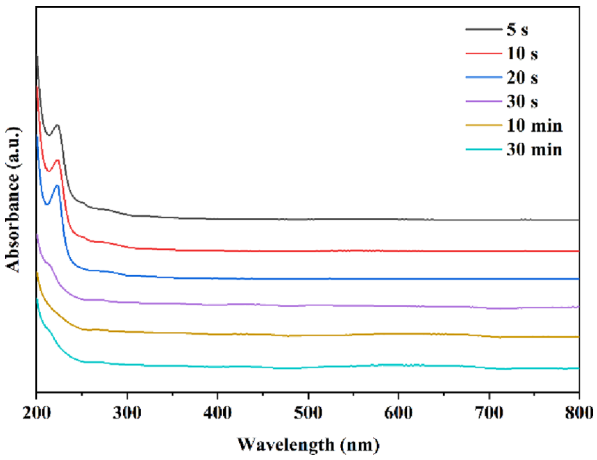

Figure 3. UV−vis absorption spectra of the samples prepared in different stages. The reaction conditions were the same as those shown in Figure 1.

displaying a lattice spacing of 0.2489 nm, which corresponds to the (111) planes of face-centered cubic (fcc) gold.[18]

The corresponding electron diffraction patterns were then obtained. As shown in Figure 1f, the diffraction point can be labeled as (111) with axial diffraction. In addition, diffracted spots attributed to reflections from the {220} (triangular box) and 1/3 {422} (box) Bragg planes were observed in the SAED pattern of the sample. Thus, it can be speculated that the flat surface of the microplate was parallel to the (111) plane. In addition, another set of weaker reflection points was observed at 1/3 {422}, which is generally considered to be forbidden by fcc single-crystal structures or caused by the presence of twin boundaries.[19]

X-ray diffraction (XRD) was used to characterize the crystal structures of the Au microplates. There were five diffraction peaks at 38.18, 44.38, 64.57, 77.56, and 81.72° corresponding to the (111), (200), (220), (311), and (222) crystal faces, respectively (JCPDS no. 04-0784) (Figure 2). In particular, the diffraction peak of the (111) lattice plane was significantly more intense than the other diffraction peaks, indicating that the (111) lattice plane was the base plane. Furthermore, compared to the standard PDF card combined with the diffraction spots in Figure 1f, we believe that the Au microplates are single crystals. Additionally, there were no other visible peaks in the XRD pattern, which proved that the synthesized Au microplates had a high crystallinity and purity.

To investigate the development process of the Au microplates in the current system, the evolution of the UV−vis spectra of the samples obtained at different stages was monitored (Figure 3). The strong absorption peak at approximately 220 nm was assigned to the interband transition of the conduction band electrons, which corresponds to the absorption band of the Au^{3+} ions.[11,20,21] The peak at approximately 220 nm gradually decreased after 30 s and nearly disappeared after 10 min, indicating that there were fewer Au ions in the reaction solution. Upon further increasing the reaction time, the baseline of the spectrum shifted from the beginning due to Rayleigh scattering, indicating that some particles were produced and suspended in the solution. In addition, a broad spectral band was observed at wavelengths greater than 500 nm.[22−24] Because these plasmon bands beyond 500 nm were not sharp or wide, this means not only that the microstructure did have plasmon dipole oscillations but also that its shape deviated from the spherical structure to a large extent, and its size distribution was broad,[25−28] implying the final generation of Au microplates.

To further explore the micromorphology of various samples obtained during the reaction process, we examined normal and negatively stained TEM images of samples selected based on the UV−vis results (Figures 4 and 5). Figure 4a illustrates the morphology of pure cellulose gel, providing evidence for the highly stable association of solvents and HEC molecules, ensuring the stability of the HEC aqueous solution.[29] From Figure 4b,c, it is evident that the Au nanoparticles are uniformly dispersed in the HEC matrix.

The rich hydroxyl groups on HEC molecules can combine with Au ions, which can promote electron transfer from HEC to Au ions, eventually reducing them to Au atoms. Over time, the reduced Au atoms aggregated to form small, uniform spherical Au nanoparticles. After the addition of H_2O_2, the Au nanoparticles exhibited initial growth stages accompanied by the formation of small twinned crystals (Figure 5a,b). As the reaction time increased further, we observed typical polygonal particles accompanied by a corresponding increase in size (Figure 5c−e). When the reaction time reached 30 min, we observed micrometer-sized trigonal and hexagonal Au microplates (Figure 5f).

Vibrational spectroscopy is a powerful tool for investigating the local properties of materials. To study the role of the HEC in the current system, we utilized Fourier transform infrared (FTIR) spectroscopy to obtain spectra. However, in infrared absorption experiments, particularly in aqueous systems, samples can be limited by water absorption interference. To overcome this limitation, we prepared a HEC/Au microplate composite in solid form by transferring the colloidal solution to a Petri dish. After being dried overnight at 303 K, the prepared

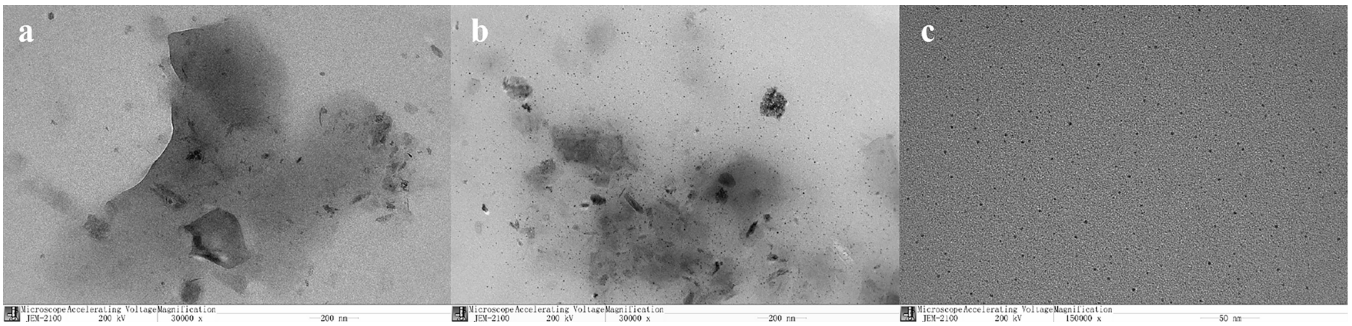

Figure 4. Negative staining TEM images of HEC and the HEC/HAuCl4 mixture. (a) HEC and (b, c) HEC/$HAuCl_4$ mixture after it had been allowed to stand overnight at 298 K.

https://doi.org/10.1021/acsomega.3c06039
ACS Omega 2024, 9, 8789−8796

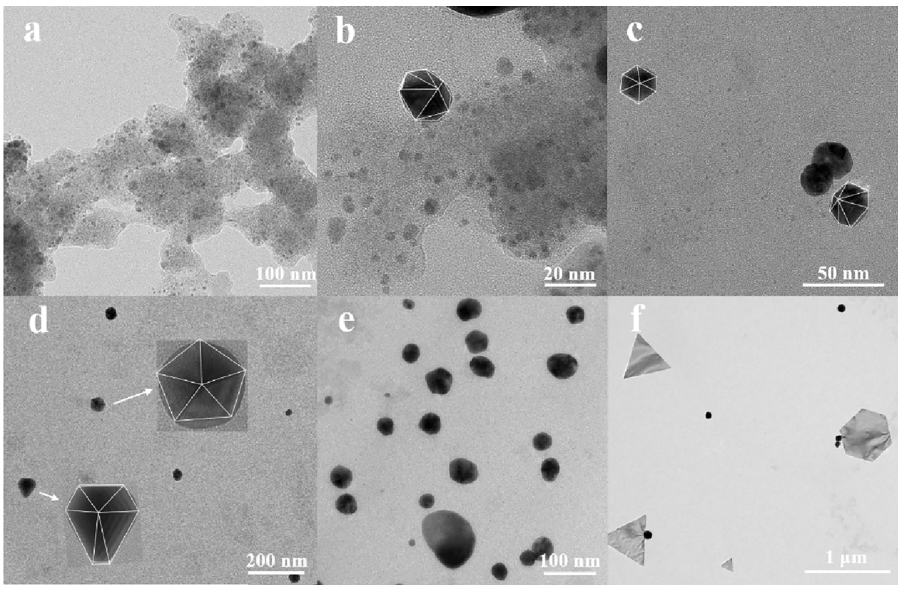

Figure 5. TEM/HRTEM images of Au microplates prepared at different stages: (a) 5 s; (b) 10 s; (c) 20 s; (d) 30 s; (e) 10 min; and (f) 30 min. The reaction conditions were the same as those shown in Figure 1.

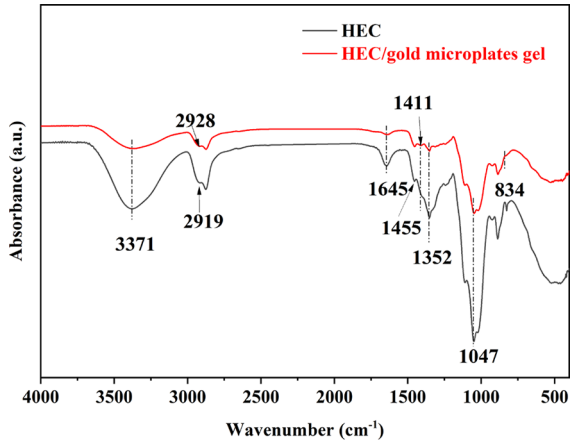

Figure 6. FTIR spectra of HEC and the HEC/gold microplate gel in the solid form. The solid form of the HEC/gold microplate gel was acquired immediately after a 6 h reaction, without undergoing further washing or purification. Instead, it was dried overnight at 303 K.

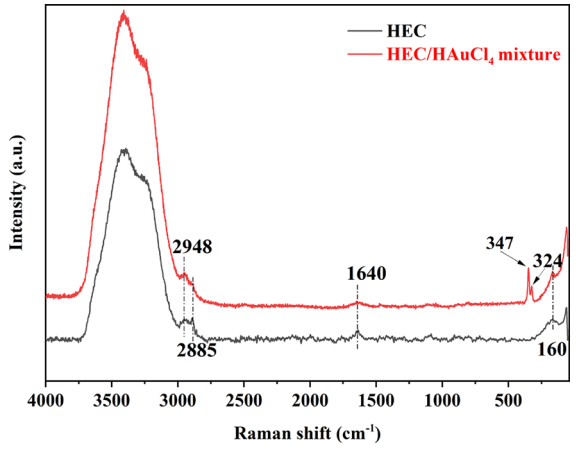

Figure 7. Raman spectra of the HEC/$HAuCl_4$ mixtures. The mixture was then incubated overnight at 298 K.

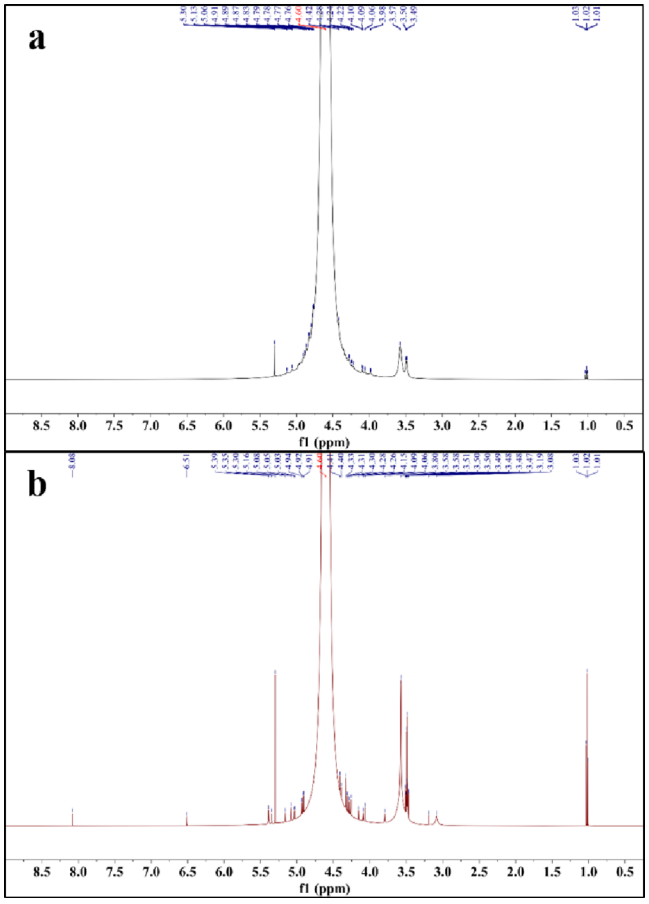

Figure 8. ^1H NMR spectra of HEC and gold microplates. (a) HEC and (b) HEC/gold microplate gel. The HEC/gold microplate gel was obtained immediately after 6 h of reaction without further washing or purification with deionized water.

powder was subjected to FTIR analysis. To prevent phase separation during the IR experiments, we carefully controlled the heating rate to ensure that the HEC/Au microplate gel

https://doi.org/10.1021/acsomega.3c06039
ACS Omega 2024, 9, 8789−8796

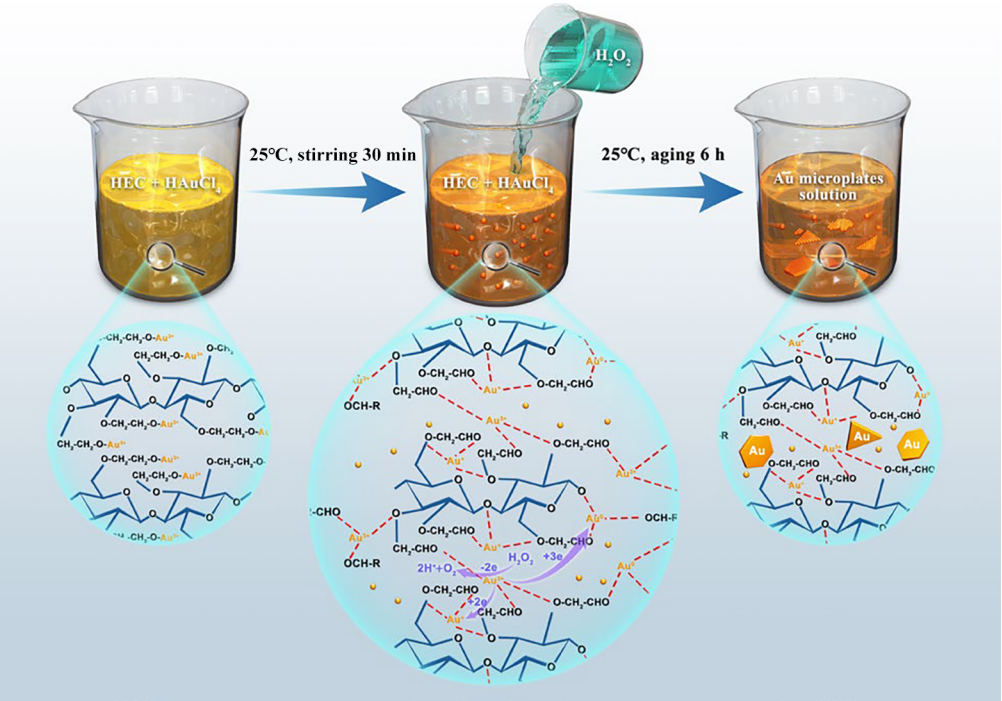

Figure 9. Schematic illustration of the possible growth mechanism of gold microplates.

remained clear without any signs of turbidity. As a precaution, we kept the drying temperature below 318 K, and we are confident that all spectra were obtained from samples without phase separation.[30,31]

Figure 6 shows the FTIR spectra of the HEC and HEC/Au microplates. The spectrum of HEC displays distinct peaks corresponding to various functional groups, including the stretching of hydrogen bonds O−H and C−H at 3371 and 2919 cm^{-1}, the carbonyl and carboxyl double bond stretching at 1645 cm^{-1}, and the O−H hydrogen bending at 1047 cm^{-1}. Additionally, peaks at 1455 and 1352 cm^{-1} are attributed to the in-plane bending of C−H (wiggle of CH═CH and CH_2).[32−34] Likewise, the same characteristic peaks were evident at 3371, 2928, 1645, and 1047 cm^{-1} for the HEC/Au microplates, confirming the involvement of aldehydes and OH groups in the production and stabilization of Au microplates.[35] The broadening of the band in the region of wavenumbers of 3700−3000 cm^{-1} reveals that the hydroxyl groups are not free and undergo a different mode of hydrogen bonding, characterized by polymeric association, resulting in weaker bonded OH groups.[36] In addition, a broad and distinct band in the 1222−950 cm^{-1} region is observed in the spectrum of HEC, which is a characteristic of the stretching vibrations of C−O−C. In contrast, when examining the HEC-Au microplates, it was observed that the O−H stretching vibration was weak, the absorption peak intensity of the C−H stretching vibration was low, and the intensities of the absorption bands at 1352 and 1047 cm^{-1} were significantly reduced. In addition, the spectrum showed bands attributed to the C═O stretching vibration in the range 1660−1560 cm^{-1}, bands in the range 1467−1400 cm^{-1}, and bands in the range 947−844 cm^{-1}. The bands of 1467−1400 cm^{-1} are assigned to the CH_2 symmetric bending and rocking vibrations, respectively, wheresa the bands of 936−844 cm^{-1} are attributed to the CH rocking vibration.

Raman spectroscopy offers distinct advantages when recording cellulose spectra. This is because a highly polar bond system generates intense infrared bands but has comparatively low polarizability, thus causing water to possess a very weak Raman spectrum that does not interfere with the cellulose spectrum. Raman spectroscopy was used to further investigate the aqueous system of the HEC/$HAuCl_4$ composite and accurately represent the vibrational motion and characteristic vibrational transitions in our study (Figure 7). In the Raman spectrum of HEC, the OH stretching vibration occurred in the region 3200−3500 cm^{-1}, with the same frequency as in the infrared spectrum but with a significantly higher intensity. The most intense band around 2885 cm^{-1} is likely due to the methyl protons. Furthermore, the infrared band in the 1100−1000 cm^{-1} range, corresponding to ring-framework vibrations involving C−O ring stretching,[37,38] shows a decrease in intensity, indicating that the ring becomes more constrained (or less free) in the gel state. The band intensities of the CH, CH_2, and COH groups,[39,40] which correspond to the internal deformation vibration band in the range of 1200−1700 cm^{-1}, decreased as gelation occurred, indicating the impact of the gelation process on $AuCl_4^-$. However, the fact that the band does not completely disappear in the gel state suggests that some $AuCl_4^-$ groups remain coordinated with water molecules when the gel is formed. The most significant spectral change between the sol and gel state is observed in the frequency range 200−500 cm^{-1}, with all bands in this region becoming sharper after gelation. This spectroscopic behavior suggests that $HAuCl_4$ primarily interacts with the side chains of HEC and does not significantly affect the glucose ring. These findings are consistent with previous IR spectroscopy findings.

To identify the chemical structures of the HEC and HEC/Au microplates, ^1H NMR spectroscopy was performed. In Figure 8a, the signals detected at 3.49−3.57 and 4.6−4.8 ppm from the spectral data are attributed to methylene protons and water, respectively,.[32,41] In contrast, for the HEC/Au micro-

https://doi.org/10.1021/acsomega.3c06039
ACS Omega 2024, 9, 8789−8796

plate composite, except for the signal of aldehyde molecules at 8.08 ppm, the above-mentioned HEC signals were all present and detected (Figure 8b).[42] This result confirms the reduction reaction between the HEC and Au ions.

As shown in Figure 9, it is known that HEC is rich in hydroxyl functional groups in both the main cellulose chain and hydroxyethyl side chains. Because of its high molecular weight and the formation of hydrogen bonds with water molecules, HEC creates a thick solution when dissolved in water.[43] This solution swells to form a porous gel-like structure with a substantial surface area,[44] which can serve as a template for growing gold nanostructures.[45] When $HAuCl_4$ is mixed with the HEC matrix, Au ions are captured and immobilized on the negatively charged hydroxyl groups (−OH) on the HEC polymer chains to form coordination bonds. Then, the hydroxyl groups on HEC undergo oxidation, transforming into carbonyl groups. During this process, a small portion of the gold ions is reduced to Au^+ or even elemental gold (Au^0).[46] Simultaneously, the addition of H_2O_2 facilitates the reduction of the Au3+ or Au+ ions that are immobilized on the hydroxyl or carbonyl groups, present both in the main cellulose chain and in the hydroxyethyl side chain. This accelerates the generation of Au atoms. These continuously formed Au atoms are subsequently deposited on the surface of the Au nuclei. Because of the anisotropic growth properties of the Au crystals and the confinement effect of the HEC matrix structure, the resulting elemental Au eventually self-assembles into microplates characterized by their distinct flat polygonal shape.

In summary, our results suggest that HEC acts as a nanoscale structure-directing agent and provides weak reductive sites for Au ions, whereas H_2O_2 acts as a reductive enhancer, promoting the generation of Au microplates under mild conditions. In addition, the presence of HEC in the system not only helps to prepare Au microplates but also enhances their biocompatibility and water solubility. This makes the HEC-directed synthesis of Au microplates a potentially useful approach for various biomedical applications.

CONCLUSIONS

In summary, this study is the first to report a simple and environmentally friendly method using HEC and H_2O_2 for the synthesis of flat polygonal Au microplates. Based on the experimental results, it is believed that HEC should act both as a nanoscale structure-directing agent and as a weak reducing site in the system, whereas H_2O_2 acts as a reductive enhancer to accelerate the reaction under mild conditions. This ultimately facilitates the self-assembly of Au nuclei into microplates with a distinct flat polygonal shape.

ASSOCIATED CONTENT

Supporting Information

The Supporting Information is available free of charge at https://pubs.acs.org/doi/10.1021/acsomega.3c06039.

Samples prepared under various reaction conditions and SEM images of different samples (PDF)

AUTHOR INFORMATION

Corresponding Author

Hongwei Yang − *State Key Laboratory of Advanced Technologies for Comprehensive Utilization of Platinum Metals, Kunming Institute of Precious Metals, Kunming 650106, People's Republic of China; Yunnan Precious Metal Laboratory Co. Ltd., Kunming 650106, People's Republic of China*; orcid.org/0000-0002-0674-1024; Email: nanolab@ipm.com.cn

Authors

Linlin He − *State Key Laboratory of Advanced Technologies for Comprehensive Utilization of Platinum Metals, Kunming Institute of Precious Metals, Kunming 650106, People's Republic of China*

Bo Shen − *State Key Laboratory of Advanced Technologies for Comprehensive Utilization of Platinum Metals, Kunming Institute of Precious Metals, Kunming 650106, People's Republic of China*

Yu Ren − *State Key Laboratory of Advanced Technologies for Comprehensive Utilization of Platinum Metals, Kunming Institute of Precious Metals, Kunming 650106, People's Republic of China; Yunnan Precious Metal Laboratory Co. Ltd., Kunming 650106, People's Republic of China*

Huaming Mao − *State Key Laboratory of Advanced Technologies for Comprehensive Utilization of Platinum Metals, Kunming Institute of Precious Metals, Kunming 650106, People's Republic of China; Yunnan Precious Metal Laboratory Co. Ltd., Kunming 650106, People's Republic of China*

Jungang Yin − *State Key Laboratory of Advanced Technologies for Comprehensive Utilization of Platinum Metals, Kunming Institute of Precious Metals, Kunming 650106, People's Republic of China; Yunnan Precious Metal Laboratory Co. Ltd., Kunming 650106, People's Republic of China*

Wei Dai − *State Key Laboratory of Advanced Technologies for Comprehensive Utilization of Platinum Metals, Kunming Institute of Precious Metals, Kunming 650106, People's Republic of China; Yunnan Precious Metal Laboratory Co. Ltd., Kunming 650106, People's Republic of China*

Shuanglong Zhao − *State Key Laboratory of Advanced Technologies for Comprehensive Utilization of Platinum Metals, Kunming Institute of Precious Metals, Kunming 650106, People's Republic of China; Yunnan Precious Metal Laboratory Co. Ltd., Kunming 650106, People's Republic of China*

Complete contact information is available at: https://pubs.acs.org/10.1021/acsomega.3c06039

Author Contributions

Linlin He: Writing − original draft, Conceptualization, Methodology, Investigation, Writing − review and editing. Bo Shen: Methodology, Investigation. Yu Ren: Investigation. Huaming Mao: Investigation. Jungang Yin: Investigation, Validation. Wei Dai: Investigation, Validation. Shuanglong Zhao: Validation. Hongwei Yang: Project administration, Supervision, Writing − review & editing.

Notes

The authors declare no competing financial interest.

REFERENCES

(1) Live, L. S.; Murray-Methot, M.-P.; Masson, J.-F. Localized and propagating surface plasmons in gold particles of near-micron size. *J. Phys. Chem. C* **2009**, *113* (1), 40−44.

(2) Yang, L.; Zhou, Z.; Song, J.; Chen, X. Anisotropic nanomaterials for shape-dependent physicochemical and biomedical applications. *Chem. Soc. Rev.* **2019**, *48* (19), 5140−5176.

(3) Su, S.; Zou, M.; Zhao, H.; Yuan, C.; Xu, Y.; Zhang, C.; Wang, L.; Fan, C.; Wang, L. Shape-controlled gold nanoparticles supported on MoS 2 nanosheets: Synergistic effect of thionine and MoS_2 and their application for electrochemical label-free immunosensing. *Nanoscale.* **2015**, *7* (45), 19129−19135.
(4) Singh, A. V.; Batuwangala, M.; Mundra, R.; Mehta, K.; Patke, S.; Falletta, E.; Patil, R.; Gade, W. N. Biomineralized anisotropic gold microplate−macrophage interactions reveal frustrated phagocytosis-like phenomenon: a novel paclitaxel drug delivery vehicle. *ACS Appl. Mater. Interfaces.* **2014**, *6* (16), 14679−14689.
(5) Zhang, Y.; Zhan, X.; Xiong, J.; Peng, S.; Huang, W.; Joshi, R.; Cai, Y.; Liu, Y.; Li, R.; Yuan, K.; Zhou, N.; Min, W. Temperature-dependent cell death patterns induced by functionalized gold nanoparticle photothermal therapy in melanoma cells. *Sci. Rep.* **2018**, *8* (1), 8720.
(6) Ogiso, M.; Kobayashi, J.; Imai, T.; Matsuoka, K.; Itoh, M.; Imamura, T.; Okada, T.; Miura, H.; Nishiyama, T.; Hatanaka, K.; Minoura, N. Carbohydrate immobilized on a dendrimer-coated colloidal gold surface for fabrication of a lectin-sensing device based on localized surface plasmon resonance spectroscopy. *Biosens. Bioelectron.* **2013**, *41*, 465−470.
(7) Xu, Z.; Shi, X.; Jiang, H.; Song, Y.; Zhang, L.; Wang, F.; Du, S.; Chen, J. A general method to regenerate arrayed gold microelectrodes for label-free cell assay. *Anal. Biochem.* **2017**, *516*, 57−60.
(8) Byranvand, M. M.; Kharat, A. N. One pot green synthesis of gold nanowires using pomegranate juice. *Mater. Lett.* **2014**, *134*, 64−66.
(9) Liu, H.; Yang, Q. A two-step temperature-raising process to gold nanoplates with optical and surface enhanced Raman spectrum properties. *CrystEngComm.* **2011**, *13* (7), 2281−2288.
(10) Chen, L.; Hu, H.; Liu, Q.; Ji, F.; Chen, S.; Xu, Y.; Zhang, Q. Halide-free synthesis of Au nanoplates and monitoring the shape evolution process through a marker experiment. *J. Mater. Chem. C* **2016**, *4* (27), 6457−6460.
(11) Pienpinijtham, P.; Han, X. X.; Suzuki, T.; Thammacharoen, C.; Ekgasit, S.; Ozaki, Y. Micrometer-sized gold nanoplates: starch-mediated photochemical reduction synthesis and possibility of application to tip-enhanced Raman scattering (TERS). *Phys. Chem. Chem. Phys.* **2012**, *14* (27), 9636−9641.
(12) Xin, W.; Yang, J.-M.; Li, C.; Goorsky, M. S.; Carlson, L.; De Rosa, I. M. Novel strategy for one-pot synthesis of gold nanoplates on carbon nanotube sheet as an effective flexible SERS substrate. *ACS Appl. Mater. Interfaces.* **2017**, *9* (7), 6246−6254.
(13) Shao, Y.; Jin, Y.; Dong, S. Synthesis of gold nanoplates by aspartate reduction of gold chloride. *ChemComm.* **2004**, *9*, 1104−1105.
(14) Yu, T.; Wu, Z.; Kim, W.-S. Mild temperature synthesis of gold nanoplates using polyethyleneimine and their improved surface enhanced Raman signal. *RSC Adv.* **2014**, *4* (71), 37516−37521.
(15) Miranda, A.; Malheiro, E.; Skiba, E.; Quaresma, P.; Carvalho, P. A.; Eaton, P.; de Castro, B.; Shelnutt, J. A.; Pereira, E. One-pot synthesis of triangular gold nanoplates allowing broad and fine tuning of edge length. *Nanoscale* **2010**, *2* (10), 2209−2216.
(16) Kida, T. Synthesis of gold nanosheets at a liquid/liquid interface using an amphiphilic polyoxometallate/surfactant hybrid photocatalyst. *Langmuir* **2008**, *24* (15), 7648−7650.
(17) Safavi, A.; Shekarnoush, M.; Ajamian, M.; Zolghadr, A. R. High-yield synthesis, characterization, self-assembly of extremely thin gold nanosheets in sugar based deep eutectic solvents and their high electrocatalytic activity. *J. Mol. Liq.* **2019**, *279*, 208−223.
(18) Chen, L.; Ji, F.; Xu, Y.; He, L.; Mi, Y.; Bao, F.; Sun, B.; Zhang, X.; Zhang, Q. High-yield seedless synthesis of triangular gold nanoplates through oxidative etching. *Nano Letters.* **2014**, *14* (12), 7201−7206.
(19) Nootchanat, S.; Thammacharoen, C.; Lohwongwatana, B.; Ekgasit, S. Formation of large H_2O_2-reduced gold nanosheets via starch-induced two-dimensional oriented attachment. *RSC Adv.* **2013**, *3* (11), 3707−3716.
(20) Cheng, Y.; Qiu, C.; Ma, H.; Zhang, X.; Gu, X. Unusual corrosion process of gold nanoplates and the mechanism study. *Nanoscale* **2010**, *2* (5), 685−688.
(21) Emam, H. E.; Zahran, M. K.; Ahmed, H. B. Generation of biocompatible nanogold using H_2O_2−starch and their catalytic/antimicrobial activities. *Eur. Polym. J.* **2017**, *90*, 354−367.
(22) Ahmed, H. B.; Abdel-Mohsen, A. M.; Emam, H. E. Green-assisted tool for nanogold synthesis based on alginate as a biological macromolecule. *RSC Adv.* **2016**, *6* (78), 73974−73985.
(23) Verma, H. N.; Singh, P.; Chavan, R. M. Gold nanoparticle: synthesis and characterization. *Veterinary world* **2014**, *7* (2), 72.
(24) Emam, H. E.; Ahmed, H. B. Carboxymethyl cellulose macromolecules as generator of anisotropic nanogold for catalytic performance. *Int. J. Biol. Macromol.* **2018**, *111*, 999−1009.
(25) Ahmed, H. B.; Zahran, M. K.; Emam, H. E. Heatless synthesis of well dispersible Au nanoparticles using pectin biopolymer. *Int. J. Biol. Macromol.* **2016**, *91*, 208−219.
(26) Link, S.; El-Sayed, M. A. Size and temperature dependence of the plasmon absorption of colloidal gold nanoparticles. *J. Phys. Chem. B* **1999**, *103* (21), 4212−4217.
(27) Link, S.; El-Sayed, M. A. Spectral properties and relaxation dynamics of surface plasmon electronic oscillations in gold and silver nanodots and nanorods. *ACS Publications* **1999**, *103*, 8410−8426.
(28) Link, S.; Wang, Z. L.; El-Sayed, M. A. Alloy formation of gold−silver nanoparticles and the dependence of the plasmon absorption on their composition. *J. Phys. Chem. B* **1999**, *103* (18), 3529−3533.
(29) Brown, W.; Henley, D.; Öhman, J. Studies on cellulose derivatives. Part II. The influence of solvent and temperature on the conFigureuration and hydrodynamic behaviour of hydroxyethyl cellulose in dilute solution. *Makromol. Chem.* **1963**, *64* (1), 49−67.
(30) Kjøniksen, A. L.; Nyström, B.; Lindman, B. Dynamic viscoelasticity of gelling and nongelling aqueous mixtures of ethyl (hydroxyethyl) cellulose and an ionic surfactant. *Macromolecules* **1998**, *31* (6), 1852−1858.
(31) Ostrovskii, D.; Kjøniksen, A. L.; Nyström, B.; Torell, L. M. Association and thermal gelation in aqueous mixtures of ethyl (hydroxyethyl) cellulose and ionic surfactant: FTIR and Raman study. *Macromolecules* **1999**, *32* (5), 1534−1540.
(32) Şen, F.; Kahraman, M. V. Preparation and characterization of hybrid cationic hydroxyethyl cellulose/sodium alginate polyelectrolyte antimicrobial films. *Polym. Adv. Technol.* **2018**, *29* (7), 1895−1901.
(33) Emam, H. E.; El-Zawahry, M. M.; Ahmed, H. B. One-pot fabrication of AgNPs, AuNPs and Ag-Au nano-alloy using cellulosic solid support for catalytic reduction application. *Carbohydr. Polym.* **2017**, *166*, 1−13.
(34) Emam, H. E.; El-Hawary, N. S.; Ahmed, H. B. Green technology for durable finishing of viscose fibers via self-formation of AuNPs. *Int. J. Biol. Macromol.* **2017**, *96*, 697−705.
(35) Goia, D. V. Preparation and formation mechanisms of uniform metallic particles in homogeneous solutions. *J. Mater. Chem.* **2004**, *14* (4), 451−458.
(36) Selim, I. Z.; Basta, A. H.; Mansour, O. Y.; Atwa, A. I. Hydroxyethyl cellulose. II. IR spectra and their relation with the dielectric properties of hydroxyethyl celluloses. *Polym. Plast Technol. Eng.* **1994**, *33* (2), 161−174.
(37) Schenzel, K.; Fischer, S. NIR FT Raman spectroscopy−a rapid analytical tool for detecting the transformation of cellulose polymorphs. *Cellulose* **2001**, *8*, 49−57.
(38) Makarem, M.; Lee, C. M.; Kafle, K.; Huang, S.; Chae, I.; Yang, H.; Kubicki, J. D.; Kim, S. H. Probing cellulose structures with vibrational spectroscopy. *Cellulose* **2019**, *26*, 35−79.
(39) Edwards, H. G. M.; Farwell, D. W.; Williams, A. C. FT-Raman spectrum of cotton: a polymeric biomolecular analysis. *Spectrochim. Acta A Mol. Spectrosc.* **1994**, *50* (4), 807−811.
(40) Gierlinger, N.; Schwanninger, M. The potential of Raman microscopy and Raman imaging in plant research. *Spectroscopy* **2007**, *21* (2), 69−89.
(41) Ibrahim, H. M.; Reda, M. M.; Klingner, A. Preparation and characterization of green carboxymethylchitosan (CMCS)−Polyvinyl

https://doi.org/10.1021/acsomega.3c06039
ACS Omega 2024, 9, 8789−8796

alcohol (PVA) electrospun nanofibers containing gold nanoparticles (AuNPs) and its potential use as biomaterials. *Int. J. Biol. Macromol.* **2020**, *151*, 821−829.
(42) Ahmed, H. B.; Attia, M. A.; El-Dars, F. M. S. E.; Emam, H. E. Hydroxyethyl cellulose for spontaneous synthesis of antipathogenic nanostructures:(Ag & Au) nanoparticles versus Ag-Au nano-alloy. *Int. J. Biol. Macromol.* **2019**, *128*, 214−229.
(43) Zhang, Y.; Jin, Q.; Zhao, J.; Wu, C.; Fan, Q.; Wu, Q. Facile fabrication of pH-sensitive core−shell nanoparticles based on HEC and PMAA via template polymerization. *Eur. Polym. J.* **2010**, *46* (7), 1425−1435.
(44) Islam, M. S.; Chen, L.; Sisler, J.; Tam, K. C. Cellulose nanocrystal (CNC)−inorganic hybrid systems: synthesis, properties and applications. *J. Mater. Chem. B* **2018**, *6* (6), 864−883.
(45) Wang, C.; Song, F.; Wang, X.-L.; Wang, Y.-Z. A cellulose nanocrystal templating approach to synthesize size-controlled gold nanoparticles with high catalytic activity. *Int. J. Biol. Macromol.* **2022**, *209*, 464−471.
(46) Emam, H. E.; El-Hawary, N. S.; Ahmed, H. B. Green technology for durable finishing of viscose fibers via self-formation of AuNPs. *Int. J. Biol. Macromol.* **2017**, *96*, 697−705.

https://doi.org/10.1021/acsomega.3c06039
ACS Omega 2024, 9, 8789−8796